Relativistic analysis of the ^{208}Pb$(e,e'p)^{207}$Tl reaction at high momentum

J. M. Udías,* P. Sarriguren, E. Moya de Guerra, and J. A. Caballero
Instituto de Estructura de la Materia, Consejo Superior de Investigaciones Científicas, Serrano 119, E-28006 Madrid, Spain
(Received 22 December 1995)

The recent ^{208}Pb$(e,e'p)^{207}$Tl data from NIKHEF-K at high missing momentum ($p_m > 300$ MeV/c) are compared to theoretical results obtained with a fully relativistic formalism previously applied to analyze data on the low missing momentum ($p_m < 300$ MeV/c) region. The same relativistic optical potential and mean-field wave functions are used in the two p_m regions. The spectroscopic factors of the various shells are extracted from the analysis of the low-p_m data and then used in the high-p_m region. In contrast to previous analyses using a nonrelativistic mean-field formalism, we do not find a substantial deviation from the mean-field predictions other than that of the spectroscopic factors, which appear to be consistent with both low- and high-p_m data. We find that the difference between results of relativistic and nonrelativistic formalisms is enhanced in the $p_m < 0$ region that will be interesting to explore experimentally.

PACS number(s): 25.30.Fj, 24.10.Jv, 21.10.Jx

Coincidence $(e,e'p)$ measurements at quasielastic kinematics have been shown to provide very detailed information on the energy and momentum distributions of the bound nucleons [1]. This is so because at quasielastic kinematics the $(e,e'p)$ reaction can be treated with confidence [1] in the impulse approximation (IA), i.e., assuming that the detected knocked out proton absorbs the whole momentum (q) and energy (ω) of the exchanged photon.

In the past $(e,e'p)$ experiments in parallel kinematics provided high precision measurements of reduced cross sections in the missing momentum range $-50 < p_m < 300$ MeV/c [2]. This range of p_m values was covered by varying the q value while maintaining $\mathbf{p}_m$ parallel to $\mathbf{q}$ (in what follows we refer to this as the low-p_m region). Recently, the range of missing momentum has been extended by $(e,e'p)$ measurements at (q,ω)-constant kinematics [3].

The new range of p_m values ($340 < p_m < 500$ MeV/c) was covered by varying the direction of the proton detector between $\sim 99°$ and $\sim 140°$, with fixed values of q (221 MeV/c) and ω (110 MeV), at an incoming electron energy of 487 MeV. We will refer to the latter as the high-p_m region. In both regions the kinetic energy of the detected proton was $T_F = 100$ MeV.

In Ref. [3] the high-p_m data for the shells $3s_{1/2}$, $2d_{3/2}$, $1h_{11/2}$, $2d_{5/2}$, and $1g_{7/2}$ in ^{208}Pb, were compared with standard nonrelativistic calculations based on the DWEEPY program developed in Ref. [4], that had also been used for the analysis of the low-p_m data. The authors of Ref. [3] conclude that the high-p_m data are substantially larger than the mean-field predictions. The purpose of this paper is to see whether this conclusion still holds when the data are analyzed with the fully relativistic formalism recently developed [5,6].

The simplest approximation to analyze the $(e,e'p)$ process is the plane wave impulse approximation (PWIA), where one also makes the assumption that the proton is ejected from the nucleus without any further interaction with the residual nucleus. In nonrelativistic PWIA the differential cross section factorizes into two terms, the elementary electron-proton cross section, accounting for the interaction between the incident electron and the bound proton, and the spectral function that accounts for the probability to find a proton with given energy and momentum in the nucleus. Although the factorization is destroyed when one takes into account the distortion of the electron and/or outgoing proton waves, it is useful and common practice to analyze the results in terms of a reduced cross section defined in such a way that would coincide with the spectral function if factorization were fulfilled. For selected values of the missing energy E_m (i.e., for selected single-particle shells) the reduced cross section is given by

$$\rho(\mathbf{p}_m) = \int_{\Delta E_m} dE_m [\sigma^{ep} |\mathbf{p}_F| E_F]^{-1} \frac{d^6\sigma}{dE_F d\epsilon_f d\Omega_F d\Omega_f}, \quad (1)$$

with $\mathbf{p}_m$ the missing momentum, $E_F, |\mathbf{p}_F|, \Omega_F$ (ϵ_f, Ω_f) the outgoing proton (electron) kinematical variables, and experimentally, the integral is evaluated over the interval ΔE_m that contains the peak of the transition under study. The term σ^{ep} represents the elementary electron-proton cross section. The experimental data of $\rho(\mathbf{p}_m)$ are obtained dividing the experimental cross section by σ^{ep}_{cc1}, as given by Eq. (17) of Ref. [7]. We therefore use the same expression for σ^{ep} in our theoretical calculations. In PWIA $\rho(\mathbf{p}_m)$ represents the momentum distribution of the selected single-particle shell. The spectroscopic factor S_α for a given α shell is determined by scaling the theoretical predictions for $\rho(\mathbf{p}_m)$ to the experimental data.

The standard nonrelativistic formalism [2] involves the DWEEPY program, which is based on an expansion of the one-body current operator to second order in the momenta, and can be schematically described as follows. The nonrelativistic wave functions for the bound and outgoing nucleons are obtained from phenomenological potentials of the Woods-Saxon type. The parameters of the Woods-Saxon potential for the bound proton are adjusted for each individual shell. The optical potential for the outgoing proton is fitted to

*Present address: Institute für Theoretische Physik. Universität Tübingen. Auf der Morgenstelle, 14. D72076 Tübingen. Germany.

TABLE I. Spectroscopic factors deduced from the relativistic and nonrelativistic analyses of the low-p_m data in the reaction ^{208}Pb$(e,e'p)^{207}$Tl. The numbers within parentheses indicate the statistical error derived from the fit.

	$3s_{1/2}$	$2d_{3/2}$	$1h_{11/2}$	$2d_{5/2}$	$1g_{7/2}$
Nonrel. (Ref. [2])	0.50	0.53	0.42	0.44	0.19
Nonrel. (Ref. [3])	0.55	0.57	0.58	0.54	0.26
Rel. (this paper and Ref. [5])	0.70(5)	0.73(5)	0.64(4)	0.60(5)	0.30(4)

elastic proton scattering data. The Coulomb distortion of the electron waves is treated in an approximate way.

The initial motivation of the fully relativistic formalism was to incorporate in an exact way the effect of the Coulomb distortion on the electron waves [5,8]. However, it was soon realized [5,6] that this formalism is also more adequate than the previous nonrelativistic one in accounting for the outgoing proton distortion.

In the relativistic treatment, the nucleons are described by solutions of the Dirac equation with scalar and vector (S-V) potentials. For the bound proton we use the TIMORA code [9]. The wave function of the outgoing proton is obtained by solving the Dirac equation with a S-V optical potential [10], fitted to elastic proton scattering data. The complete relativistic nucleon current operator with either convention [7] CC2 or CC1 is used.

Fully relativistic analyses for the quasielastic $(e,e'p)$ reaction from the shells $3s_{1/2}$ [5,8] and $2d_{3/2}$ [5] on ^{208}Pb have already been made in the low-p_m region. The values of the spectroscopic factors obtained with these relativistic analyses, $S_\alpha \simeq 0.7$, were much larger than the values obtained from previous nonrelativistic analyses ($S_\alpha \simeq 0.5$) [2]. A similar situation was found in other doubly closed shell nuclei as ^{40}Ca. In all cases considered, larger spectroscopic factors were obtained with the relativistic analyses [5,8]. The origin of this difference is discussed in detail in Ref. [6]. The larger values are consistent with theoretical predictions [11–13] as well as with the spectroscopic factors obtained from other methods [14].

In this Rapid Communication we first apply a similar relativistic analysis to the low-p_m data for the $1h_{11/2}$, $2d_{5/2}$, and $1g_{7/2}$ shells in ^{208}Pb. The spectroscopic factors resulting from this analysis, as well as the ones previously obtained [5] for the $3s_{1/2}$ and $2d_{3/2}$ shells, are then used to calculate the reduced cross section in the high-p_m region.

The method used to obtain the spectroscopic factors is as described in Ref. [5]. For each shell the overall scale factor has been obtained by means of an error weighted least-square procedure. The resulting spectroscopic factors are given in Table I for all the shells under consideration here. The numbers within parentheses correspond to the statistical error derived from the fitting procedure. In the two first rows of Table I we show the spectroscopic factors obtained from the standard nonrelativistic analyses of Refs. [2,3], which differ on the approximate treatment of the electron Coulomb distortion. Note that both nonrelativistic analyses give spectroscopic factors that are substantially smaller than ours.

We show in Figs. 1 and 2 the reduced cross sections in the p_m range -100 MeV $< p_m < 600$ MeV for the five shells in ^{208}Pb considered, scaled by the corresponding spectroscopic factors. The experimental data in the low-p_m [2] and high-p_m [3] regions are shown by small and large circles with error bars, respectively.

In the low-p_m region of Figs. 1 and 2 we show our relativistic results scaled by the spectroscopic factors given in the last row of Table I. We can see in Figs. 1 and 2 that the shape of $\rho(p_m)$ for each shell agrees very well with data in the low-p_m region. This gives confidence on the reliability of these spectroscopic factors. As indicated in the figures, these results have been obtained using the CC2 current operator. Fits of the same quality can be obtained with the CC1 operator [5]. However, the cross sections obtained with the CC1 operator in this p_m region are typically 10% larger than those obtained with CC2 and therefore the spectroscopic factors obtained are 10% smaller (see also Table II of Ref. [5]).

In the high-p_m region of Figs. 1 and 2 we compare with experiment our relativistic results obtained with the current

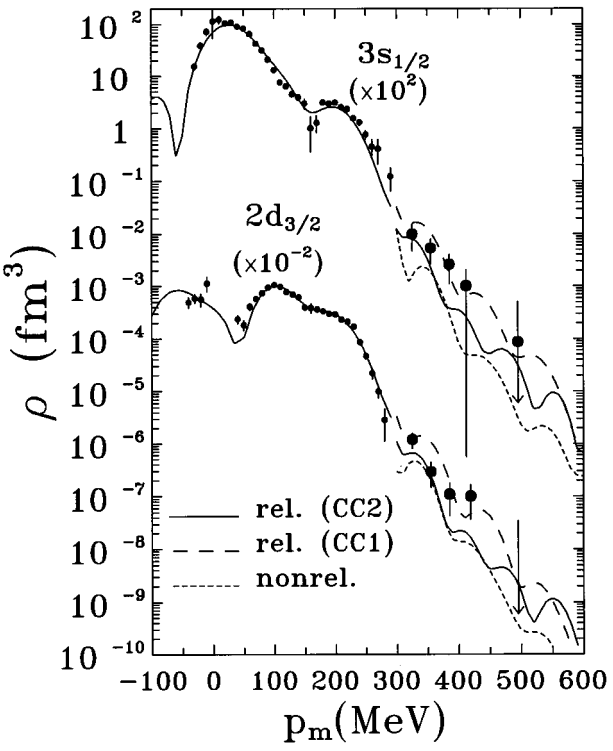

FIG. 1. Reduced cross sections versus missing momentum for the shells $3s_{1/2}$ and $2d_{5/2}$ of ^{208}Pb. In the low-p_m region we show by solid lines the relativistic results scaled with the spectroscopic factors of the last row in Table I. Small circles with error bars are data from Ref. [2]. In the high-p_m region we show the relativistic results obtained with the currents CC2 (solid lines) and CC1 (long-dashed lines), as well as the nonrelativistic results (short-dashed lines) and the experimental data from Ref. [3].

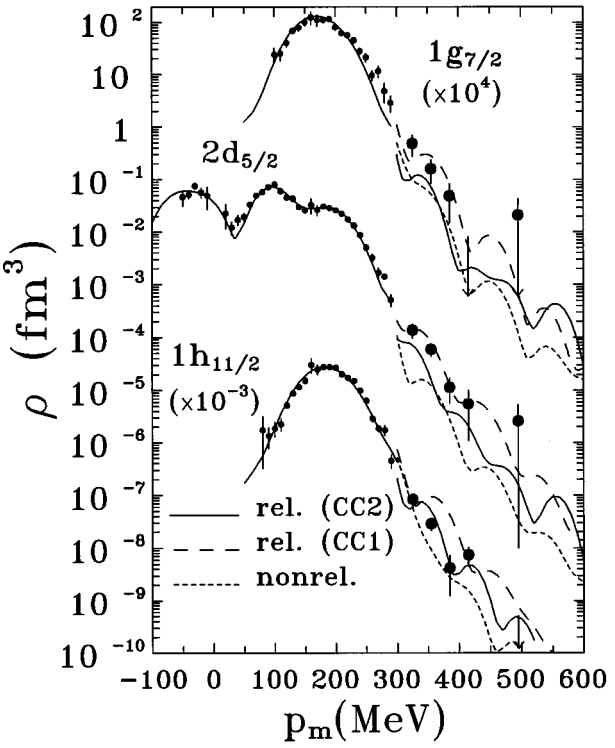

FIG. 2. Same as Fig. 1 but for the shells $1g_{7/2}$, $2d_{3/2}$, and $1h_{11/2}$.

operators CC1 and CC2 scaled by the corresponding spectroscopic factors. Note that although these two relativistic calculations give practically identical results for $\rho(p_m)$ in the low-p_m region, they can differ by as much as one order of magnitude in the high-p_m region. This difference gives also an indication of the theoretical uncertainty that can be expected in the high-p_m region even for calculations that fit equally well the low-p_m region. Also shown in these figures are the results of nonrelativistic calculations from Ref. [3].

The discontinuity at $p_m=300$ MeV in our theoretical results is due to the different kinematics (parallel or perpendicular) in the two regions. The main source of this discontinuity can be traced back to the electron Coulomb distortion and disappears in the limit of plane waves for both electron and proton. A discussion of the different effects of electron Coulomb distortion in parallel and perpendicular kinematics can be found in Ref. [5].

One can see from Figs. 1 and 2 that most of the high-p_m data lie between the predictions of the two relativistic calculations, while the nonrelativistic calculations underestimate the experimental strength. To account for the lack of strength at high-p_m in the nonrelativistic calculations, correlations were included by Bobeldijk *et al.* [3], multiplying the bound nucleon wave functions by different correlation functions. The analysis carried out by these authors showed that the calculations including the short-range correlations (SRC) and tensor correlations as prescribed by Pandharipande [13] did not modify substantially the mean-field predictions. This agrees with the conclusion of Müther and Dickhoff [15], who find that there is no significant increase due to SRC at high momentum and low excitation energy compared to the mean-field result. On the contrary, the momentum distributions calculated from quasiparticle wave functions given by Mahaux and Sartor [11], and Ma and Wambach [12] exhibit an important enhancement in the high-p_m region and tend to fit better the experimental data. This result was considered as an indication of the importance of long-range correlations.

Clearly, the relativistic results do not leave much room to claim a significant lack of strength in the mean-field predictions at the high momenta and low excitation energies considered here. This can be viewed as supporting the remarks in Ref. [16] in the sense that the relativistic nuclear models could emulate the role of correlations. Whether the effect of correlations is contained to some extent in the relativistic mean-field formalism is certainly a point that deserves further study.

It should be stressed here that we made no attempt to optimize agreement with data, and that we use a very simple relativistic nuclear model. The bound nucleon wave functions are those obtained from the TIMORA code without any further adjustment. Taking this into account, it is remarkable the good agreement with experiment found. It would be interesting to analyze the effect of using different relativistic wave functions for both the bound and the scattered proton, as well as to study the role of the low components of the Dirac wave functions in the high-momentum region. From previous studies in Refs. [6,17] we know that the effect of the enhancement of the lower components of the wave functions in the relativistic models is very small at low-p_m. There is work in progress [18] to clarify whether this is also the case in the high-p_m region.

Although the data seem to favor the results of the relativistic calculations we would like to point out that part of the lack of strength in the nonrelativistic result of Ref. [3] is due to the fact that the normalizing σ^{ep} used in the theoretical calculations is different from that used in the data. In Ref. [3] a nonrelativistic approximation ($\sigma^{ep}_{\rm NR}$) was used in the theoretical calculation of $\rho(p_m)$ rather than σ^{ep}_{cc1}. As can be seen in Fig. 3 the nonrelativistic strength in the high-p_m region is somewhat increased when σ^{ep}_{cc1} is used instead. We consider that because σ^{ep}_{cc1} has been used in the plotted data, the same expression should be used in the theoretical calculations when comparing to data.

In Fig. 3 we have also shown the negative missing momentum region. This region corresponds to a similar kinematics as the high-p_m region so far discussed except that the polar proton angle is different ($p_m>0$ corresponds to $\phi=180°$, while $p_m<0$ corresponds to $\phi=0°$). Thus, the only difference in the cross section is the sign in front of the longitudinal-transverse (LT) contribution [19], which is different in each region. One should keep in mind that if factorization were fulfilled the results in both regions should be exactly symmetric. It is interesting to observe that the relativistic results are less symmetric than the nonrelativistic ones and therefore, the deviation between the relativistic and the nonrelativistic results in the $p_m<0$ region is enhanced with respect to the one seen in the $p_m>0$ region. It would therefore be interesting to probe the $p_m<0$ region experimentally.

In conclusion, we find that compared to the standard nonrelativistic results the reduced cross sections obtained with the relativistic formalism are quenched in the low-p_m region

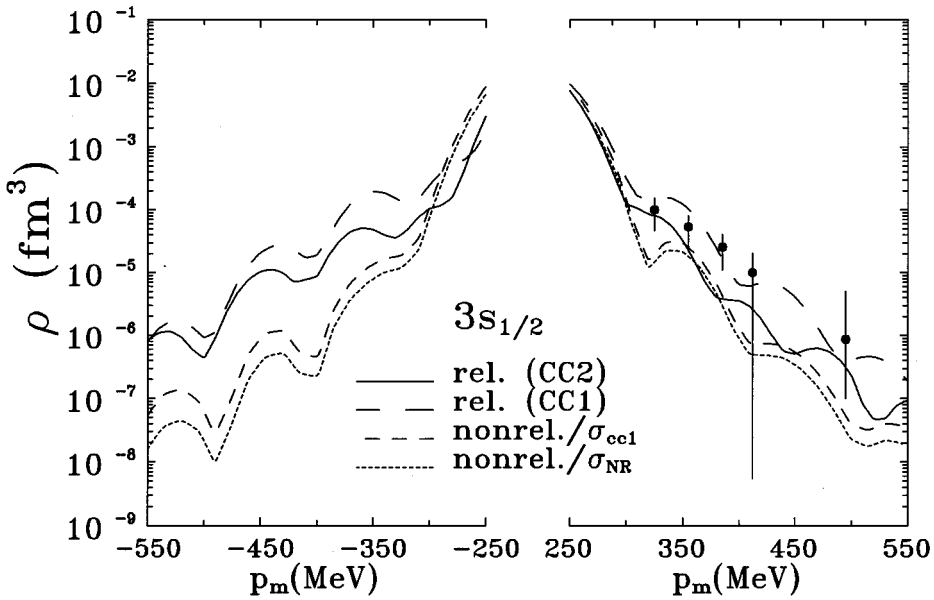

FIG. 3. Reduced cross sections for the $3s_{1/2}$ shell in both the positive and negative high-p_m regions. Circles with error bars are data from Ref. [3]. We show relativistic calculations obtained with the currents CC2 (solid lines) and CC1 (long-dashed lines), and nonrelativistic calculations normalized with σ^{ep}_{cc1} (dashed lines) and $\sigma^{ep}_{\rm NR}$ (short-dashed lines).

and enhanced in the high-p_m region for the five shells considered. The resulting spectroscopic factors are then larger and the profile of the momentum distributions agree better with experiment. A clear success of the relativistic analysis is the high quality fits to the low-p_m data found in each of the orbitals, even though the relativistic mean field and nucleon wave functions have not been adjusted to specific single-particle properties. The high-p_m data are also fairly well accounted for. From our analysis the same nucleon mean-field wave functions and spectroscopic factors describing the low-p_m data seem to be valid in the high-p_m region discussed here. We would like to emphasize that this high-p_m region is very sensitive to theoretical models, not only to relativistic or nonrelativistic approaches, correlated or uncorrelated wave functions, but also to the choice of the relativistic nucleon current operator. This choice is of prime importance since further nonrelativistic approaches depend also on it. Thus, it is desirable to have more experimental information in high missing momentum regions. Particularly interesting will be to explore the $p_m<0$ region that has been found here to depend more strongly on whether a relativistic or nonrelativistic approach is used.

We thank I. Bobeldijk for providing us with the experimental data and the nonrelativistic single-particle cross sections used in the nonrelativistic analyses of Ref. [3] and G. van der Steenhoven for useful comments about the NIKHEF-K experiments. One of us (J.M.U.) acknowledges support from the EC-program ''Human Capital and Mobility'' under Contract No. CHRX-CT 93-0323. This work was partially supported by DGICYT (Spain) under Contract No. 92/0021-C02-01.

[1] S. Frullani and J. Mougey, Adv. Nucl. Phys. **14**, 1 (1985).
[2] E.N.M. Quint, Ph.D. Thesis, University of Amsterdam, 1988.
[3] I. Bobeldijk *et al.*, Phys. Rev. Lett. **73**, 2684 (1994).
[4] C. Giusti and F. Pacati, Nucl. Phys. **A473**, 717 (1987); **A485**, 461 (1988); M. Traini, Phys. Lett. B **213**, 1 (1988); S. Boffi, C. Giusti, and F. Pacati, Nucl. Phys. **A336**, 416 (1980); C. Giusti and F. Pacati, *ibid.* **A336**, 427 (1980).
[5] J.M. Udías, P. Sarriguren, E. Moya de Guerra, E. Garrido, and J.A. Caballero, Phys. Rev. C **48**, 2731 (1993).
[6] J.M. Udías, P. Sarriguren, E. Moya de Guerra, E. Garrido, and J.A. Caballero, Phys. Rev. C **51**, 3246 (1995).
[7] T. de Forest, Jr., Nucl. Phys. **A392**, 232 (1983).
[8] Y. Jin, D.S. Onley, and L.E. Wright, Phys. Rev. C **45**, 1311 (1992).
[9] C.J. Horowitz, D.P. Murdock, and B.D. Serot, in *Computational Nuclear Physics*, edited by K. Langanke, J.A. Maruhn, and S.E. Koonin (Springer-Verlag, Berlin, 1991); C.J. Horowitz and B.D. Serot, Nucl. Phys. **A368**, 503 (1981); Phys. Lett. **86B**, 146 (1979).
[10] S. Hama, B.C. Clark, E.D. Cooper, H.S. Sherif, and R.L. Mercer, Phys. Rev. C **41**, 2737 (1990); E.D. Cooper, S. Hama, B.C. Clark, and R.L. Mercer, *ibid.* **47**, 297 (1993).
[11] C. Mahaux and R. Sartor, Adv. Nucl. Phys. **20**, 1 (1991).
[12] Z.Y. Ma and J. Wambach, Phys. Lett. B **256**, 1 (1991).
[13] V.R. Pandharipande, C.N. Papanicolas, and J. Wambach, Phys. Rev. Lett. **53**, 1133 (1984).
[14] G.J. Wagner, Prog. Part. Nucl. Phys. **24**, 17 (1990).
[15] H. Müther and W.H. Dickhoff, Phys. Rev. C **49**, R17 (1994).
[16] M. Kleinmann, R. Fritz, H. Müther, and A. Ramos, Nucl. Phys. **A579**, 85 (1994).
[17] Y. Jin and D.S. Onley, Phys. Rev. C **45**, 377 (1994).
[18] J.M. Udías, J.A. Caballero, E. Moya de Guerra, and P. Sarriguren (unpublished).
[19] A. Picklesimer and J.W. Van Order, Phys. Rev. C **40**, 290 (1989).